Editors' Suggestion | Featured in Physics

Fluid physics of telescoping cardboard boxes

Jolet de Ruiter [*,†], Emil Visby Østergaard [*], Sean Marker, and Kaare H. Jensen [‡]
Department of Physics, Technical University of Denmark, DK-2800 Kgs, Lyngby, Denmark

(Received 11 June 2021; accepted 15 February 2022; published 1 April 2022)

The economics, environmental impact, and mechanical properties of paper-based storage containers have been widely studied. However, knowledge of the physical processes relevant to the end-user experience is unavailable. This paper outlines the main effects associated with the closing and opening of telescoping boxes, which are used, for instance, to store and transport board games, footwear, mobile phones, and tablet computers. The sliding motion of the lid is controlled by the flow in a thin film of air in the gap separating the lid and the base of the box. Based on a broad comparison between theory and experiments on real and synthetic boxes, we find that the process is primarily controlled by the shape of the gap between the base and the lid. We derive a master equation for the lid motion and identify the origin of three distinct experimental regimes. Finally, an optimal design for a rapidly closing box is identified.

DOI: 10.1103/PhysRevFluids.7.044101

I. INTRODUCTION

From shipping containers to glass bottles, rigid containers are widely used to maintain product integrity during transportation and storage. Paper-based boxes, which first saw use in the late 19th century, are in particularly widespread use due to their excellent strength-to-weight characteristics, low cost, and relative ease of manufacturing [1]. The mechanics of paper, printing, and writing has been widely studied [2–5]; however, knowledge of basic physical processes that are active during the use of storage boxes is lacking. Since the quantity of units is very high, it is clear that understanding how the structural design and method of use impact the general quality of a given box is an important question.

Our focus is on telescoping boxes [Fig. 1(a)], which are particularly convenient because they allow products with different form factors to fit into a single storage unit. For instance, a single box design can accommodate products of different lengths, such as pairs of skis, umbrellas, or posters. During the closing process, the telescopic sliding motion of the lid is controlled by the flow in a thin film of air in the gap separating the lid and the base of the box. Identical physics govern thin film flows in many familiar cases, e.g., in the frames of tightly fitting doors and windows. Moreover, it is closely related to the motion of objects in constricted tubes, such as a falling cylinder viscometer [6], drops in closed capillaries [7], or rigid objects traveling through lubricated elastic tubes [8]. A defining feature of a cardboard box is that it must be securely sealed to protect the content prior to shipment. A key role is played by the lid, which must be properly sized to provide an appropriate tradeoff between safety and convenience. If the lid is loose, it may accidentally open and damage the content. However, if the lid and base fit tightly, it may become too difficult for the consumer to

[*]These authors contributed equally to this work.
[†]Present address: Agrotechnology and Food Sciences Group, Wageningen University and Research, 6700AA Wageningen, the Netherlands.
[‡]khjensen@fysik.dtu.dk

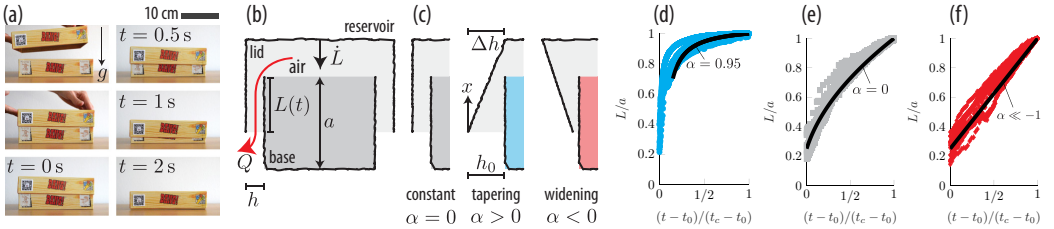

FIG. 1. Telescoping boxes. (a) Image sequence of a typical closing process and (b) conceptual sketch: air escapes the box of height a at the rate Q via the gap of width h between the lid and base. The time-dependent overlap between the lid and base is denoted $L(t)$. (c) Closeup of the gap, highlighting three distinct cases: constant, tapering, and widening corresponding to the gap form factor $\alpha = \Delta h/h_0 = 0$, $\alpha > 0$ and $\alpha < 0$, respectively, in Eq. (5). (d)–(f) Experimental data from 13 commercially available boxes (32 experiments): relative lid-base overlap L/a plotted as a function of time t scaled by the closing time t_c and initial time t_0. Solid lines represent limiting theory cases in Eq. (13), Eq. (12), and Eq. (14), respectively. [An initial overlap $L/a = \ell_0 = 0.25$ was assumed in panels (e) and (f).] See details of the data classification scheme in the text.

remove the lid. Also the time, and hence cost, required to close the lid prior to shipment or storage may still be significant. It is this closing process, and the dependence of its dynamics on physical and geometric parameters, which we seek to elucidate.

The paper is organized as follows. First, we describe our experiments on a number of different telescoping boxes. Subsequently, a theory based on laminar low-Reynolds-number fluid flow is derived. Next, the theory is compared to the telescopic box experiments and to data from idealized containers with full geometric control. Similarities to imbibition and squeeze-flow processes are highlighted, and important design trade-offs are identified, including an optimal box design which minimizes the closing time. Finally, we conclude the paper by summarizing our main results.

II. RESULTS

A. Closing dynamics of telescoping boxes

The sliding motion of telescopic lids was observed on a sample of 13 commercially available boxes (32 experiments). Specimens were selected based on availability, and with a view to covering the broadest possible range of sizes and closing characteristics. The base was placed on a flat, horizontal surface. The lid was positioned above the base and was carefully aligned. An initial overlap of $L/a = 0.15$–0.35 was used to prevent yawing, where L is the length of the overlap region and a is the height of the box [Fig. 1(b)]. Upon release at time t_0, the lid slid vertically down over the base and came to rest [Fig. 1(a)]. The entire process took 2–50 sec. See the Supplemental Material for representative examples of the lid motion [9]. Additional experimental details are provided in the Appendix.

The closing dynamics of each box is unique [Figs. 1(d)–1(f)]; however, clear patterns emerged that allow us to roughly divide the data into three categories. In one set of experiments, the lid speed diminished continuously, and a box sometimes took as much as 50 sec to fully close [Fig. 1(d)]. Other trials progressed somewhat faster but still at at a gradually diminishing pace. In this category, the lid-base overlap length L scaled approximately with the square root of time $L \sim t^{1/2}$ [Fig. 1(e); see also gray data points in Fig. 2]. In a final set of boxes, the lid slid over the base at an approximately constant speed $L \sim t$ [Fig. 1(f)]. The aforementioned trends provide an adequate description of our data. We did not identify other clear trends, related to, for instance, box size in the experiments. We did, however, observe a strong current of air emerging from the narrow gap separating the lid and base which, occasionally, resulted in a hissing sound. We estimated that the typical slit width is $h \approx 0.1$–1 mm with slight variations between the corners and the edge

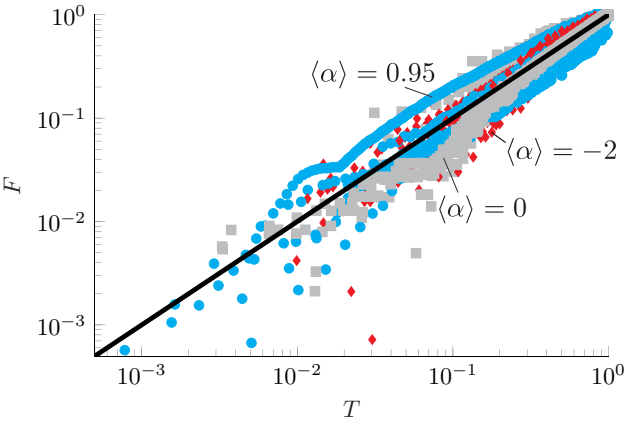

FIG. 2. Normalized lid-base overlap F [Eq. (10)] plotted as a function of normalized time T [Eq. (11)]. Data from Figs. 1(d)–1(f) are in reasonable accord with theory (solid black line) using the fitted shape factor $\langle\alpha\rangle$; see Table I.

centers. Finally, it is worth noting that we did, occasionally, observe a yawing motion of the lid as it descended. This, however, could be largely eliminated by carefully controlling the initial condition.

The maximum lid speed $\dot{L}$, based on our observations, is $\dot{L} \approx 2$ cm/sec. For a 20 cm $\times$ 20 cm box of surface area $A \approx 400\,\mathrm{cm}^2$ and gap height $h \approx 1$ mm, the mean speed of the air in the gap is $v_{\max} = A\dot{L}/(wh) \approx 1$ m/s, where $w \approx 80$ cm is the perimeter of the box. This corresponds to a maximum Reynolds number $\mathrm{Re} = \rho v h/\eta = \rho \dot{L} A/w\eta = 50$, where $\eta = 2 \times 10^{-5}$ Pa s is the viscosity of air. Because the Reynolds number $\mathrm{Re} < 50$ is relatively small, it is reasonable to assume that the fluid motion in the gap is not too far removed from ideal Stokes flow conditions. Moveover, the typical pressure generated by the weight of the lid is $\Delta p = g\rho \approx 9.8\,\mathrm{m\,s}^{-2} \times 0.1\,\mathrm{kg\,m}^{-2} \approx 1$ Pa, where g is the acceleration due to gravity and ρ is the area density of the lid; hence compression effects are negligible.

B. Theory of telescoping boxes

To rationalize the experimental observations, and elucidate the origin of the three distinct experimental regimes, we develop a simple model of the lid motion. Our theory is based on the hypothesis that the sliding process is controlled by the flow in a thin film of air in the gap separating the lid and base of the box. The weight of the lid pressurizes the gas in the box which is then forced out through the slit. The lid motion is thus directly linked to the thin-film flow by mass conservation. (Note that a similar approach was used by Clément *et al.* [10] in an investigation of shells penetrating in into granular materials. They observed air trapped below the shell escaping through the porous sand matrix, which, in some cases, is fluidized.)

The weight of the lid creates a pressure difference $\Delta p = mg/A$ between the inside of the box and the surrounding atmosphere. Here m is the mass of the lid, g is gravity, and A is the surface area of the box. This drives an air current $Q = \Delta p/R$ across the gap, where R is the hydraulic resistance of the gap, a quantity that depends on the gap geometry and the material properties of air. Mass conservation dictates the relationship between the flow rate Q, the surface area A, and the overlap length L, i.e., $Q = A\dot{L}$. The motion of the lid continues until the box is closed at $L(t_c) = a$, where a is the height of the box and t_c is the closing time. (We assume here that the lid and base are of equal height; if that is not the case the parameter a is the minimum of the height of the base and the height of the lid.) The goal of the following analysis is to determine an analytical expression for the overlap $L(t)$ as function of time t and the system parameters.

We first consider the simplest case in which the gap thickness $h = h_0$ is constant [Fig. 1(b)]. From the Hagen-Poiseuille law for low-Reynolds-number pressure-driven flow in a shallow channel, we find that the flow rate Q is

$$Q = \frac{\Delta p}{R} = \frac{h_0^3 w}{12\eta}\frac{\Delta p}{L(t)}. \tag{1}$$

Here we assume that the walls of the channel are quasistatic, while in practice, one is slowly moving downwards. The vertical speed of the lid, typically of order 5 mm/s, however, is substantially smaller than the air flow speed ($\approx$1 m/s, see above), thus lending credence to this approximation. Proceeding with our analysis of the lid motion, we use volume conservation, i.e., $Q = A\dot{L}$, which leads to

$$\frac{dL^2}{dt} = \frac{h_0^3 w \Delta p}{6A\eta}, \tag{2}$$

such that the relation between the overlap L and time t is

$$L^2 - L_0^2 = \frac{h_0^3 w \Delta p}{6A\eta}(t - t_0), \tag{3}$$

where L_0 is the (initial) overlap at $t = t_0$. Equation (3) predicts a square-root relationship between the overlap length and time, i.e., $L \sim t^{1/2}$, which is consistent with the data in Fig. 1(e). The speed of the lid diminishes over time because the length of the overlap, and hence the resistance to flow, increases over time. We note that Eq. (3) is conceptually similar to the Lucas-Washburn equation describing capillary imbibition in a slit where the flow driven by a constant capillary pressure drop is impeded by a flow path of increasing length [11,12]. The time required to close the box is

$$t^* = \frac{6A\eta a^2}{h_0^3 w \Delta p}, \tag{4}$$

where $a = L(t^*)$ is the height of the box, i.e., the final overlap length. We note that the closing time t_c scales inversely with the lid's mass m (i.e., $t_c \sim 1/\Delta p \sim 1/m$), in reasonable accord with experiments (Fig. 5).

Although the $L \sim t^{1/2}$ dependence is consistent with some of our data, this functional form does not adequately describe the remaining features in our experiments [Figs. 1(d)–1(f)]. To try to understand why some lids slide faster or slower, we now develop a more detailed model of the gap geometry. A visual inspection of the boxes revealed some variation in the lid dimensions along the vertical axis. This implies that the lid and base walls might not always be perfectly parallel. Although the precise gap height profile is unknown, it is clear from the h^3 dependence in the Hagen-Poiseuille equation (1) that even a minute change in h could strongly impact the sliding dynamics.

To account for the experimental observations (Fig. 1), we consider a linearly varying channel height profile [Fig. 1(c)]

$$h(x) = h_0\left(1 - \frac{\Delta h}{h_0}\frac{x}{a}\right) = h_0\left(1 - \alpha\frac{x}{a}\right) \tag{5}$$

valid for $0 < x < L$, where the distance x is measured upwards from the leading edge of the translating lid, h_0 is the constant gap height at $x = 0$, and Δh is the difference in height along the channel. The mean gap height is $\bar{h} = h_0 - \Delta h/2$. The geometric factor $\alpha = \Delta h/h_0$ quantifies the relative change in gap aperture [Fig. 1(c)]. It is an important parameter in the analysis, and we will now outline its main characteristics. For parallel walls, $\Delta h = 0$ and $\alpha = 0$. In a tapering channel ($\Delta h > 0$), the difference is never larger than h_0, otherwise the lid would touch the base before closing. Consequently, the permitted range is $0 < \alpha < 1$. In contrast, if the gap is widening

($\Delta h < 0$), the aperture is always wider near the top of the lid than at the leading edge, corresponding to $-\infty < \alpha < 0$.

Returning to the lid's sliding motion, we now consider the hydraulic resistance of the gap for the linear height profile in Eq. (5). Because the channel aspect ratio $h/L \sim 0.01$ and the effective Reynolds number $(h/L)^2\mathrm{Re} < 0.5$ are both relatively small, we use Stokes' equations and the lubrication approximation thereof to describe the dynamics [13]. This leads to the hydraulic resistance

$$R = \frac{12\eta}{w}\int_0^L \frac{1}{h(x)^3}\,dx, \tag{6}$$

which, for constant h, leads to Eq. (1). Using the volume conservation relation $A\dot{L} = \Delta p/R$ and introducing the dimensionless variables

$$\ell = \frac{L}{a}, \quad \tau = \frac{t}{t^*}, \quad \text{and} \quad \alpha = \frac{\Delta h}{h_0} \tag{7}$$

leads to an equation for the temporal evolution of the nondimensional overlap ℓ:

$$\frac{1}{\alpha}\frac{d\ell}{d\tau} = [(1-\ell\alpha)^{-2} - 1]^{-1}. \tag{8}$$

The solution to Eq. (8) is

$$\frac{1}{\alpha^2}\left[\frac{1}{1-\alpha\ell} - \frac{1}{1-\alpha\ell_0} - \alpha(\ell-\ell_0)\right] = \tau - \tau_0, \tag{9}$$

where ℓ_0 is the initial position at time τ_0. Rescaling Eq. (9) by the closed state [Eq. (9) with $\ell(\tau_c) = 1$, where τ_c is the closing time] leads us to define the generalized overlap function

$$F = \frac{\frac{1}{1-\alpha\ell} - \frac{1}{1-\alpha\ell_0} - \alpha(\ell-\ell_0)}{\frac{1}{1-\alpha} - \frac{1}{1-\alpha\ell_0} - \alpha(1-\ell_0)} = T, \tag{10}$$

where the relative time

$$T = \frac{\tau - \tau_0}{\tau_c - \tau_0} = \frac{t - t_0}{t_c - t_0} \tag{11}$$

is independent of t^* and hence the specific material parameters of the box [Eqs. (4) and (7)]. We can infer from Eq. (10) that the characteristics of the lid motion depends on only the magnitude of the geometric parameter $\alpha = \Delta h/h_0$. When α is small, relevant to the straight channel with parallel boundaries, we find

$$\ell^2 \approx \ell_0^2 + \left(1-\ell_0^2\right)T, \tag{12}$$

consistent with Eq. (3) and the observed $L \sim \sqrt{t}$ dynamics in Fig. 1(e). For intermediate values of $\alpha \approx 1$, corresponding to a gradually tapering channel [Fig. 1(c)], and when $\ell \to 1$ we have

$$\ell \approx \frac{1}{\alpha}\left(1 - \frac{1-\alpha}{T}\right). \tag{13}$$

Notably, this is consistent with the data in Fig. 1(d). Finally, when $\alpha \ll -1$ (the widening channel) we predict a linear motion

$$\ell \approx \ell_0 + (1-\ell_0)T, \tag{14}$$

in reasonable accord with the data in Fig. 1(f). A complete data collapse can be obtained by plotting the scaled overlap F [Eq. (10)] as function of T [Eq. (11)] and the geometric parameter $\alpha = \Delta h/h_0$. Here we have chosen $\alpha = 0.95$ for the data in Fig. 1(d), $\alpha = 0$ for Fig. 1(e), and $\alpha = -2$ for Fig. 1(f), although the precise values of α are of course unknown. With these assumption the reduced

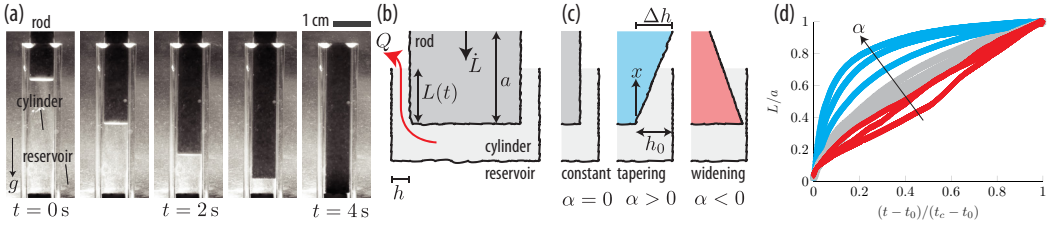

FIG. 3. Controlled experiments. (a) Image sequence of a 7.8 mm diameter 3D printed rod penetrating an 8 mm inner diameter plexiglas cylinder. (b) Conceptual sketch: the weight of the rod causes liquid to escape the cylinder of height a at the rate Q via the gap of width h. The time-dependent overlap between the rod and cylinder is denoted $L(t)$. (c) Closeup of the gap, highlighting three distinct cases: constant, tapering, and widening corresponding to $\alpha = \Delta h/h_0 = 0$, $\alpha > 0$, and $\alpha < 0$, respectively, in Eq. (5). The image sequence in panel (a) represents the $\alpha = 0$ case. (d) Experimental data: relative lid-base overlap L/a plotted as a function of time t scaled by the closing time t_c and initial time t_0 for rods. The gap shape parameter α varies from $\alpha = -13.6$ to 0.9.

overlap F is indeed proportional to T for the majority of our data, spanning almost three decades (Fig. 2).

C. Controlled experiments

It is evident from Eq. (9) that the gap shape parameter $\alpha = \Delta h/h_0$ is the main determinant of the closing process. However, in the experiments on commercially available boxes we were unable to either accurately measure or control this quantity. To mitigate this fundamental difficulty in validating our model, we conducted experiments on an analogous system with full control of the lid and base geometries [Figs. 3(a), 6, and Table II]. Straight and widening rods were fabricated using a 3D printer (see the Appendix). A rod was subsequently positioned above a wider plexiglass cylinder submerged in a larger water bath. After careful alignment along the centerline of the cylinder, the rod was released and the motion was tracked. This arrangement corresponds to the box base sliding into the lid, but otherwise the situation is equivalent to the case shown in Fig. 1.

By varying the rod geometry [Fig. 3(c)], we swept the parameter space from $\alpha = 0.9$ (a tapering gap) across $\alpha = 0$ (straight gap) to $\alpha = -13.6$ (widening gap). The data are in qualitative and quantitative accord with the predictions of Eq. (10) with no free parameters (Fig. 4). Interestingly, this explains the three experimental regimes observed in the telescoping box experiments [Figs. 1(d)–1(f)], confirming that a linearly varying gap height profile h leads precisely to these distinct behaviors. This leads to the following physical interpretation: When the gap width h is constant and $\alpha = 0$ we recover the $L \sim t^{1/2}$ Lucas-Washburn behavior because the hydraulic resistance scales linearly with the overlap length [11,12]. If, instead, the gap gradually widens, the majority of the viscous friction will be localized to a short region of length $Lh_0/\Delta h$ near the thin leading edge of the gap. This implies that the hydraulic resistance is approximately constant and consequently that the overlap scales linearly with time, i.e., $L \sim t$. Finally, when the gap is tapering, the hydraulic resistance of the gap increases and the motion continues to slow [cf. Eq. (13)], similar to squeeze flow dynamics [14].

We end our analysis of telescopic flows by considering a basic optimization problem: we seek the box which closes in the shortest amount of time. To constrain the analysis, we consider a box with constant average gap height $\bar{h}$ and linearly varying gap profile. In this system, the base height h_0 in Eq. (5) can be written as $h_0 = \bar{h} + \Delta h/2$. The system dynamics is then dictated by the nondimensional parameter $\beta = \Delta h/\bar{h}$, which defines the taper. Note that β varies in the range $-2 < \beta < 2$, otherwise the gap height h would become negative at either $x = 0$ or $x = a$ [Eq. (5)]. With these assumptions, the closing time can be deduced from Eq. (9) by solving for τ_c, that is the

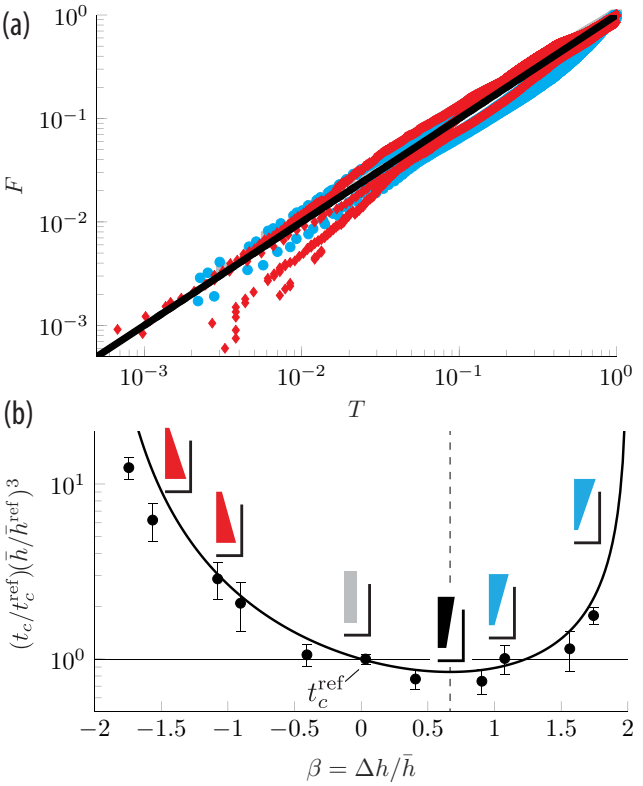

FIG. 4. (a) Normalized overlap lid-base overlap F [Eq. (10)] plotted as a function of normalized time T [Eq. (11)] for the controlled experiments. Data from Fig. 3(d) are in good accord with theory (solid black line). Error bars represent two standard deviations (5–10 repetitions). (b) Closing time t_c as function of $\beta = \Delta h/\bar{h}$ normalized by the closing time for the reference geometry (Table II) and mean gap height $\bar{h}$, in reasonable agreement with Eq. (15) (thick solid line). The dashed vertical line indicates the optimal values $\beta = 2/3$ where t_c is reduced by ∼15% when compared to the straight gap $\beta = 0$.

point of closing ($\ell = 1$). (Additional steps are outlined in the Appendix.) This leads to

$$t_c = \left(\frac{6A\eta a^2}{w\bar{h}^3\Delta p}\right)\frac{1}{\beta^2}\left[\frac{1}{1-\beta/2} - \frac{1}{1+\beta/2} - \frac{\beta}{(1+\beta/2)^2}\right], \tag{15}$$

where we recognize the prefactor as the closing time for a flat gap $h(x) = \bar{h}$; cf. Eq. (4). The predictions of Eq. (15) are in reasonable accord with data [Fig. 4(b)]. Notably, Eq. (15) predicts the existence of a local minimum when $\beta = \Delta h/\bar{h} = 2/3$ (or equivalently $\alpha = 1/2$) where the closing time is reduced by approximately 15%, to $t_c = 27\bar{t}^*/32 \approx 0.84\bar{t}^*$ when compared to the straight box. The opening angle in the optimal configuration is $\theta \approx \Delta h/a = 2\bar{h}/(3a)$. For a typical box ($a = 10\,\mathrm{cm}$ and $\bar{h} = 0.5\,\mathrm{mm}$) it is $\theta \approx 0.03 \approx 2^\circ$. This optimal box has another simple characteristic: the broadest gap $h_{\max} = h(0) = 4/3\bar{h}$ is exactly twice as wide as the narrow point $h_{\min} = h(a) = 2\bar{h}/3$. The physical origin of this optimum again lies in the h^{-3} dependence on the hydraulic resistance R [Eq. (6)].

III. DISCUSSION AND CONCLUSION

This paper has outlined the main physical effects that impact the operation of telescopic boxes. Based on a broad comparison between theory and experiments on real and synthetic boxes, we

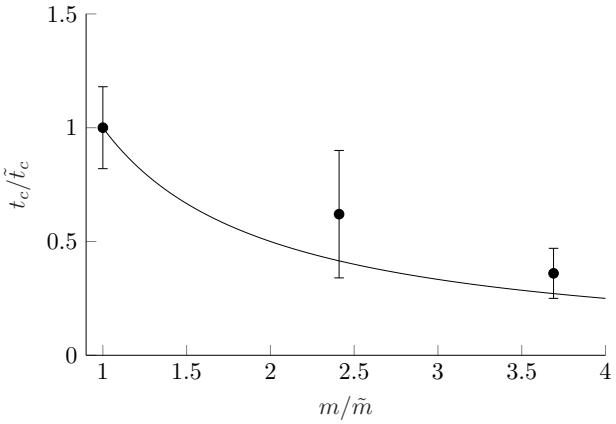

FIG. 5. Lid speed increases with mass. Closing time t_c plotted as a function of the lid mass m for the board game Photosynthesis (dots; see Table I). The solid line illustrates the approximately inverse relation (i.e., $t_c \sim 1/m$) between the two parameters. The initial mass of the lid $\tilde{m} = (199 \pm 2)\,\mathrm{g}$ was modified by adding weights to the top of the box. The mean closing time of the virgin container was $\tilde{t}_c = 2.5\,\mathrm{s}$. Error bars indicate the standard deviation.

found that the process is controlled primarily by the shape of the gap between base and the lid. Because the overlapping region increases in length over time, the relation between shape, kinetics, and closing time is highly nonlinear. If, however, the gap shape function $h(x)$ varies linearly we find that the process can be described using the geometric parameter $\alpha = \Delta h/h_0$, which quantifies the relative change in gap size across the height of the box. Finally, the optimal design for rapidly closing telescoping boxes was determined.

We speculate that the dynamics contained in the master equation (10) could be of relevance to product designers. Similarly, fabrication of the optimal box might be of interest to the packing industry. Moreover, physically analogous systems such as thin-film flows in door and window cracks and piston seals are governed by the same equations and hence follow similar design criteria. Although we have focused on a specific linear gap geometry that creates three distinct experimental regimes, it is clear that important questions for future research remain. For instance, considering an arbitrary height profile $h(x)$ could, in principle, further shorten the closing time. We also note a potentially important qualitative difference between the closing and opening processes. During the sealing of a box, the weight of the lid provides the force that increases the pressure inside the container relative to the atmosphere. The situation, however, is reversed when the box is opened, e.g., by lifting it completely off the table. In this case, the force is generated by the weight of the contents of the box and the pressure inside the container is lower than atmospheric. This, in itself, does not alter the conclusions of our study. However, if the contents of the box are sufficiently heavy, the pressure drop could lead to an (elastic) deformation of the gap geometry, hence further restricting flow.

ACKNOWLEDGMENTS

This work was supported by research grants from VILLUM FONDEN (Grant No. 37475) and the Independent Research Fund Denmark (Grants No. 9064-00069B and No. 9040-00349B).

TABLE I. Telescoping box samples corresponding to the overlap L vs time t data plotted in Figs. 1(d)–1(f). The the inferred gap aspect ratio $\langle\alpha\rangle$ was used in Fig. 2 to facilitate a comparison to Eq. (10).

Fig. 1 panel	Product name	$\langle\alpha\rangle$
f	Bang	−2
f	Brains	−2
e	Carcassone De Uitbreiding	0
f	Carcassonne Rad van Fortuin	−2
e	Catan	0
e	Codenames Pictures	0
e	Exit the Game	0
d	iPad	0.95
d	iPad Pro	0.95
f	iPhone	−2
d	MacBook Air	0.95
f	Munchkin Koethulu	−2
e	Photosynthesis	0

APPENDIX: MATERIALS AND METHODS

1. Materials and experimental methods

This section provides a detailed description of the telescoping experiments. The paper-based samples used are listed in Table I, and the setup is shown in Fig. 1(a): the base of a telescopic box was placed on a flat, horizontal surface. The lid was positioned above the base and is carefully aligned before it is released. The alignment and release were done by hand. We found this method superior to a prototype mechanically triggered release system. Upon release, the lid slid vertically down over the base before coming to rest. The entire process took 2–50 sec. A digital camera (Nikon, Japan) captured 25 images per second of the sliding process, and the position of the lid relative to the base is obtained by tracking the motion of a QR code attached to the lid. This allowed us to quantify the length of the overlapping region L between the lid and base as function of time t [Figs. 1(d)–1(f) and 5].

In addition to commercially available telescoping boxes, we conducted experiments with full control of the lid and base geometries. Solid rods of length $a = 60$ mm were 3D printed (Ultimaker 3, Ultimaker, the Netherlands). A rod was positioned above a plexiglass cylinder of inner diameter $D = 8$ mm and submerged in a large water bath. After careful alignment along the centerline of the

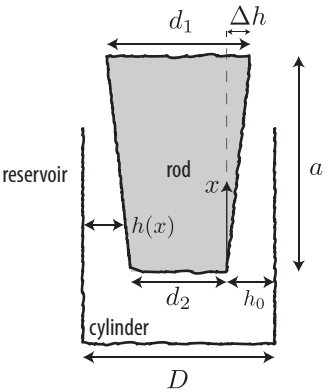

FIG. 6. Geometric parameters in the controlled experiments.

TABLE II. Parameters used in the controlled experiments shown in Figs. 3(d) and 4. Lengths d_1, d_2, $h_0 = (D - d_2)/2$, $\Delta h = (d_1 - d_2)/2$, $\bar{h} = h_0 - \Delta h/2$ are measured in mm; see Fig. 6. The inner diameter of the cylinder $D = 8$ mm and the rod length $a = 60$ mm were constant in all experiments. The first row was used as reference geometry in Fig. 4(b).

d_1	d_2	h_0	Δh	$\bar{h}$	$\alpha = \Delta h/h_0$	$\beta = \Delta h/\bar{h}$
7.40	7.38	0.31	0.01	0.31	0.03	0.03
7.55	7.32	0.34	0.12	0.28	0.34	0.41
7.74	7.31	0.35	0.22	0.24	0.62	0.91
7.76	7.20	0.40	0.28	0.26	0.70	1.08
7.89	7.10	0.45	0.40	0.25	0.88	1.56
7.93	6.98	0.51	0.48	0.27	0.93	1.74
7.38	7.40	0.30	−0.01	0.31	−0.03	−0.03
7.32	7.55	0.23	−0.12	0.28	−0.51	−0.41
7.31	7.74	0.13	−0.22	0.24	−1.65	−0.91
7.20	7.76	0.12	−0.28	0.26	−2.33	−1.08
7.10	7.89	0.06	−0.40	0.25	−7.18	−1.56
6.98	7.93	0.04	−0.48	0.27	−13.6	−1.74

cylinder, the rod was released. The vertical motion of the rod, driven by gravity, was tracked using a digital camera (see above). In the experiments, we varied the shape of the rod by modifying the linearly varying diameter $d(x) = d_1 + (d_2 - d_1)x/a$. Here d_1 and d_2 mm are the diameters at either end of the rod and x is the distance along the rod (Fig. 6 and Table II). This provided full control of the gap thickness $h(x) = D - d(x)$; cf. Eq. (5).

2. Theory of rapidly closing telescoping boxes

This section is dedicated to deriving Eq. (15), which describes the relation between the closing time t_c and the ratio of the height variation Δh to the mean channel height $\bar{h}$, which we denote $\beta = \Delta h/\bar{h}$. The relation between this quantity and the gap geometry parameter previously introduced is $\alpha = \beta/(1 + \beta/2)$. We begin by considering the dimensional closing time $t_c = \tau_c t^*$. This can be obtained from Eq. (9), using that the final overlap is equal to the box height a, i.e., $\ell(\tau_{\text{close}}) = 1$. This leads to

$$t_c = \frac{t^*}{\alpha^2}\left(\frac{1}{1-\alpha} - 1 - \alpha\right), \tag{A1}$$

where we have assumed that the initial time τ_0 and overlap ℓ_0 are both zero. It is clear that the closing time t_c increases when the gap itself is small, since $t^* \sim h_0^{-3}$ and $\alpha = \Delta h/h_0$. The situation is different, however, if we keep the average gap height $\bar{h} = h_0 - \Delta h/2$ constant. Equation (5) then implies that the leading edge gap height $h(0) = h_0$ is

$$h_0 = \bar{h}\left(1 + \frac{\beta}{2}\right), \tag{A2}$$

where $\beta = \Delta h/\bar{h}$ defines the amount of taper. Note that $-2 < \beta < 2$, otherwise the gap height h becomes negative at either $x = 0$ or $x = a$ [Eq. (5)]. Substituting Eq. (A2) into (A1) leads to (15).

[1] M. Levinson, *The Box: How the Shipping Container Made the World Smaller and the World Economy Bigger* (Princeton University Press, Princeton, 2008).

[2] A. A. Batista, The mechanics of bending a strip of paper, Eur. J. Phys. **41**, 065009 (2020).

[3] J. Kim, M.-W. Moon, K.-R. Lee, L. Mahadevan, and H.-Y. Kim, Hydrodynamics of Writing with Ink, Phys. Rev. Lett. **107**, 264501 (2011).
[4] Z. Aboura, N. Talbi, S. Allaoui, and M. Benzeggagh, Elastic behavior of corrugated cardboard: Experiments and modeling, Composite Struct. **63**, 53 (2004).
[5] T. Garbowski, T. Gajewski, and J. K. Grabski, The role of buckling in the estimation of compressive strength of corrugated cardboard boxes, Materials **13**, 4578 (2020).
[6] P. Bridgman, The effect of pressure on the viscosity of forty-three pure liquids, Proc. Am. Acad. Arts. Sci. **61**, 57 (1926).
[7] M. Vuckovac, M. Backholm, J. V. Timonen, and R. H. Ras, Viscosity-enhanced droplet motion in sealed superhydrophobic capillaries, Sci. Adv. **6**, eaba5197 (2020).
[8] B. Rallabandi, J. Eggers, M. A. Herrada, and H. A. Stone, Motion of a tightly fitting axisymmetric object through a lubricated elastic tube, J. Fluid Mech. **926**, A27 (2021).
[9] See Supplemental Material at http://link.aps.org/supplemental/10.1103/PhysRevFluids.7.044101 for representative videos of the lid motion.
[10] R. Clément, S. C. du Pont, M. Ould-Hamouda, D. Duveau, and S. Douady, Penetration and Blown Air Effect in Granular Media, Phys. Rev. Lett. **106**, 098001 (2011).
[11] M. Reyssat, L. Courbin, E. Reyssat, and H. A. Stone, Imbibition in geometries with axial variations, J. Fluid Mech. **615**, 335 (2008).
[12] J.-B. Gorce, I. J. Hewitt, and D. Vella, Capillary imbibition into converging tubes: Beating Washburn's law and the optimal imbibition of liquids, Langmuir **32**, 1560 (2016).
[13] L. G. Leal, *Advanced Transport Phenomena: Fluid Mechanics and Convective Transport Processes*, Cambridge Series in Chemical Engineering (Cambridge University Press, Cambridge, 2007).
[14] H. Bruus, *Theoretical Microfluidics*, Oxford Master Series in Physics, Vol. 18 (Oxford University Press, Oxford, 2008).